Title

In Vivo Imaging of Retinal Oxidative Stress Using a Reactive Oxygen Species–Activated Fluorescent ProbeImaging of Retinal Oxidative Stress Using H-800CW

Journal

Investigative Ophthalmology & Visual Science, 56(10)

ISSN

0146-0404

Authors

Prunty, Megan C
Aung, Moe H
Hanif, Adam M
et al.

Publication Date

2015-09-08

DOI

10.1167/iovs.15-16810

Peer reviewed

In Vivo Imaging of Retinal Oxidative Stress Using a Reactive Oxygen Species–Activated Fluorescent Probe

Megan C. Prunty,[1] Moe H. Aung,[1] Adam M. Hanif,[2] Rachael S. Allen,[2] Micah A. Chrenek,[1] Jeffrey H. Boatright,[1,2] Peter M. Thule,[3,4] Kousik Kundu,[*,5] Niren Murthy,[6] and Machelle T. Pardue[1,2]

[1]Department of Ophthalmology, Emory University, Atlanta, Georgia, United States
[2]Atlanta VA Center for Visual and Neurocognitive Rehabilitation, Atlanta, Georgia, United States
[3]Biomedical Research, Atlanta VA Medical Center, Atlanta, Georgia, United States
[4]Department of Medicine, Emory University, Atlanta, Georgia, United States
[5]LI-COR, Lincoln, Nebraska, United States
[6]Department of Bioengineering, University of California, Berkeley, California, United States

Correspondence: Machelle T. Pardue, Research Service (151 Oph), Atlanta VA Medical Center, 1670 Clairmont Rd, Decatur, GA 30033, USA;
mpardue@emory.edu.

Current affiliation: *Nalco-Champion, An Ecolab Company, Houston, Texas, United States.

Submitted: March 5, 2015
Accepted: July 30, 2015

Citation: Prunty MC, Aung MH, Hanif AM, et al. In vivo imaging of retinal oxidative stress using a reactive oxygen species–activated fluorescent probe. *Invest Ophthalmol Vis Sci*. 2015;56:5862–5870. DOI:10.1167/iovs.15-16810

Purpose. In vivo methods for detecting oxidative stress in the eye would improve screening and monitoring of the leading causes of blindness: diabetic retinopathy, glaucoma, and age-related macular degeneration.

Methods. To develop an in vivo biomarker for oxidative stress in the eye, we tested the efficacy of a reactive oxygen species (ROS)–activated, near-infrared hydrocyanine-800CW (H-800CW) fluorescent probe in light-induced retinal degeneration (LIRD) mouse models. After intravitreal delivery in LIRD rats, fluorescent microscopy was used to confirm that the oxidized H-800CW appeared in the same retinal layers as an established ROS marker (dichlorofluorescein).

Results. Dose–response curves of increasing concentrations of intravenously injected H-800CW demonstrated linear increases in both intensity and total area of fundus hyperfluorescence in LIRD mice, as detected by scanning laser ophthalmoscopy. Fundus hyperfluorescence also correlated with the duration of light damage and functional deficits in vision after LIRD. In LIRD rats with intravitreal injections of H-800CW, fluorescent labeling was localized to photoreceptor inner segments, similar to dichlorofluorescein.

Conclusions. Hydrocyanine-800CW detects retinal ROS in vivo and shows potential as a novel biomarker for ROS levels in ophthalmic diseases.

Keywords: oxidative stress, fluorescent probes, retinal degeneration

Reactive oxygen species (ROS), such as hydroxyl radicals and superoxides, contribute to numerous ophthalmic diseases, including age-related retinal degeneration,[1,2] glaucoma,[3] and diabetic retinopathy (DR).[4,5] While these retinal diseases have different pathophysiologies, they share the characteristic of ROS overproduction that overwhelms inherent antioxidant mechanisms of the neurons and supporting glial cells, leading to a cascade of oxidative stress that contributes to retinal damage.[6] Animal models of retinal degeneration demonstrate that oxidative stress contributes to photoreceptor death in retinitis pigmentosa,[7] light-induced retinal degeneration,[8,9] and natural aging.[10] Consistent with this, antioxidant treatments slow the rate of retinal degeneration by protecting against ROS.[10–12] Within the retina, mitochondria inherently generate the largest quantities of ROS as a byproduct of adenosine triphosphate (ATP) production.[13] In the context of glaucoma and diabetes mellitus, mitochondrial dysfunction contributes to ROS production,[14,15] which subsequently exerts oxidative stress on retinal ganglion cells,[16] photoreceptors,[17] and retinal microvasculature.[18]

Since oxidative stress is a common factor causing retinal dysfunction, in vivo detection of ROS could prove a valuable diagnostic tool for many ophthalmic diseases. In addition, ocular ROS could be used to detect brain disorders and systemic diseases that have ocular phenotypes,[19] such as stroke,[20,21] Alzheimer's disease,[22,23] and diabetes.[5,15,17,24] However, high reactivity and extremely short half-lives of superoxide and hydroxyl radicals, on the order of 10^{-6} and 10^{-9} seconds, respectively,[25] make measurement difficult. Currently, ROS quantification is limited to ex vivo approaches, such as spectrofluorometric determinations of dichlorofluorescein (DCF, a fluorescent probe that reacts intracellularly with peroxidase),[26] histologic detection of dihydroethidium (DHE),[27] and high-performance liquid chromatography (HPLC) for a wide variety of oxidants (e.g., hydrogen peroxide, superoxide, or nitric oxide[28]). However, these methods all have limited clinical applicability. High-performance liquid chromatography and DCF require tissue biopsy, and DHE spontaneously autoxidizes and rapidly photobleaches.[27] To circumvent the instability of ROS, it is common to measure downstream products of antioxidant mechanisms (proteins such as superoxide dismutase) or quantify the damage to DNA, RNA, lipids, and proteins caused by oxidative stress. Although oxidative stress byproducts are more stable and easier to quantify, they do not directly measure ROS and, again, cannot be measured in vivo. Recently, a reversibly responsive,

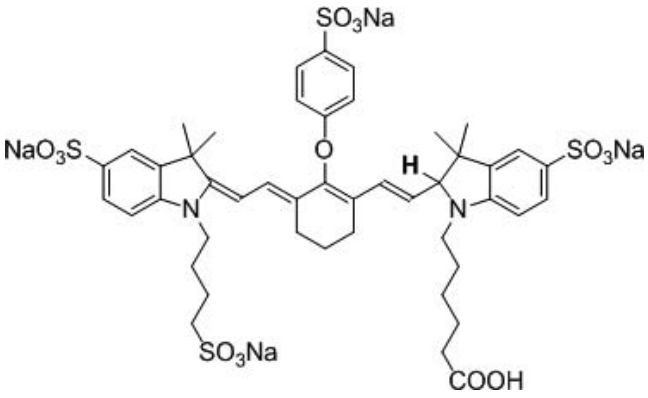

Figure 1. Molecular structure of hydrocyanine-800CW (H-800CW).

profluorescent nitroxide probe was reported for detection of retinal oxidative stress in a rat model of ischemia.[29] This probe offers the ability to detect and visualize oxidative stress in vivo in the retina, although the sensitivity to small ROS changes may be limited.

Hydrocyanine sensors have been used for highly sensitive quantification of ROS generation.[30] When these hydrocyanine molecular probes are oxidized by superoxide or hydroxyl radicals, they irreversibly convert from a nonfluorescent hydrocyanine into a fluorescent cyanine molecule (Fig. 1). Within the hydrocyanine family there are probes with different emission wavelengths; these have been established for use in cell culture[31] and ex vivo.[32] Hydrocyanine-800CW (H-800CW) is a new hydrocyanine, which has physical/chemical properties similar to those of the previously published hydrocyanine-indocyanine green (H-ICG). Hydrocyanine-800CW oxidizes into 800CW, which has excitation and emission maxima at 774 nm and 789 nm, similar to indocyanine green (ICG). Kundu et al.[30] have shown that H-ICG is nontoxic in cell culture experiments, even at extremely high doses, and no toxic side effects have been noted in animal models.

Although hydrocyanines have been used in imaging ROS in vivo in different animal models,[20,33–40] their clinical applications are limited because of low tissue penetration of optical probes and the lack of suitable noninvasive instruments. Optical imaging of H-800CW in the eye is a more practical and clinically relevant application, as the eye is transparent and as suitable clinical instruments, that is, fundus cameras and scanning laser ophthalmoscopes with ICG filters, are already available. Indocyanine green is already FDA approved for imaging retinal vasculature and is routinely used in the clinic. Therefore, the potential for successful clinical ocular application of H-800CW seems high. Here, we tested H-800CW's ability to quantify ROS generated in vivo within the retina after light-induced retinal degeneration (LIRD). We used both systemic and intravitreal administration of the probe to show potential clinical use and test sensitivity to detect retinal ROS at different concentrations and levels of retinal damage.

Methods

Animals and Experimental Design

All procedures were approved by the Atlanta VA Institutional Animal Care and Use Committee and conformed to the ARVO Statement for the Use of Animals in Ophthalmic and Vision Research. All animals used in the study were housed on a 12:12 hour light:dark cycle with chow and water provided ad libitum. Long Evans rats (300–350 g) and 129/SvJ mice (23–30 g) were obtained from Charles River (Wilmington, MA, USA). Animals were randomly divided into control (CTRL) and LIRD groups. Using mice, we established a dose–response curve by testing different concentrations of H-800CW and determined the sensitivity of the ROS probe to retinal injury by exposing mice to different durations of toxic light damage. In mice, changes in visual function were quantified by optokinetic tracking (OKT), while changes in retinal function were assessed with electroretinography (ERG). In rats, we demonstrated tissue-targeted administration of H-800CW with intravitreal injections and examined retinal cross sections to determine the location of the ROS probe.

Light-Induced Retinal Damage

Light-induced retinal damage is an acute model of retinal degeneration with a well-described oxidative stress response.[41] After dilating the pupils with atropine sulfate ophthalmic solution (1%), animals were exposed to either dim (100 lux, CTRL) or bright light (60,000 lux, LIRD). The luminance of the light-emitting diode light panels was measured using a lux meter (Traceable Dual Range Light Meter; VWR International, Radnor, PA, USA). Mice were exposed for 6 hours, whereas rats were exposed for 4 hours. During light exposure, animals were singly housed in a shoebox-style cage, provided wet food ad libitum, and monitored for signs of stress (Chrenek, et al. *IOVS* 2013;54:ARVO E-Abstract 44). During bright light exposure, temperatures inside the box ranged from 29°C to 31°C.

To determine the sensitivity of H-800CW to detect varying severities of retinal injury, 129/SvJ mice were randomly assigned to either LIRD or CTRL groups. The LIRD mice were exposed to durations of 0, 1, 2, 4, or 6 hours of light damage. Control mice were not subjected to bright light. Immediately after treatment, both LIRD and CTRL mice were anesthetized and injected intravenously with H-800CW (20 mg/kg) or vehicle (0.9% NaCl). Animals were then housed in darkness prior to imaging, as described below.

Administration and Imaging of the Fluorescent Probe

At the conclusion of light exposure, mice were anesthetized with ketamine (80 mg/kg) and xylazine (16 mg/kg) and body temperature was maintained at 37°C via a heating pad. Hydrocyanine-800CW (ROSstar 800CW; LI-COR, Lincoln, NE, USA) dye was injected intravenously via penile vein at 2.5, 5, 10, or 20 mg/kg to both CTRL and LIRD mice. For the rat experiments, anesthesia was induced with ketamine (60 mg/kg) and xylazine (7.5 mg/kg), and H-800CW or vehicle was delivered intravitreally at a dose of 2 μL (10.7 nmol) per eye to both CTRL and LIRD rats.

After administration of H-800CW, all animals received yohimbine (2 mg/kg) to reverse the effects of xylazine and prevent corneal ulcers.[42,43] For the next 48 hours, animals were housed in complete darkness to prevent photobleaching while the oxidized H-800CW complexes accumulated in the eye. Two days after H-800CW injection, animals were anesthetized (as described above) and prepared for scanning laser ophthalmoscope (SLO) imaging by anesthetizing corneas with 0.5% tetracaine hydrochloride ophthalmic solution (Alcon, Fort Worth, TX, USA) and inducing mydriasis with 1% tropicamide eye drops (Bausch+Lomb, Tampa, FL, USA). The cornea was kept hydrated with a custom-made contact lens (X-cel Contacts-A Walman Company, Duluth, GA, USA) and

artificial tears (Refresh Celluvis Tears; Allergan, Inc., Irvine, GA, USA).[44] An SLO (HRA+OCT; Heidelberg, Carlsbad, CA, USA) was used to visualize oxidized H-800CW in vivo with the ICG filter. After completing fundus images with the ICG filter, a subset of LIRD and CTRL animals received an intraperitoneal injection of 1 μL 10% fluorescein (AK-Fluor 10%; Akorn, Decatur, IL, USA) to determine the integrity of retinal capillaries at this 48-hour time point.

Optokinetic Tracking Testing

Visual function was tested in mice 1 day prior to light damage using a virtual optokinetic system (OptoMotry system; Cerebral Mechanics, Lethbridge, Canada).[45–48] Optokinetic tracking testing was performed 6 days after light damage. In brief, vertical sine wave gratings were presented in a virtual drum, rotating at a speed of 12°/s. For visual acuity assessment, the spatial frequency of the grating started at 0.042 cyc/deg with 100% contrast and increased in a staircase paradigm. The maximum spatial frequency that elicited a head tracking response was determined with the OptoMotry software and considered the spatial frequency threshold.

Electroretinography

Seven days after LIRD and following overnight dark adaptation, mice were anesthetized under dim red light with ketamine (80 mg/kg) and xylazine (16 mg/kg) for ERG recordings, as previously described.[12,49,50] For these experiments, a gold wire loop acted as the active electrode by contacting the cornea through a layer of 1% methylcellulose (Allergan, Inc.). To reference and ground the active electrode recordings, needles were placed bilaterally on the cheeks and on the tail, respectively. Flash stimuli of increasing intensity were presented using a Ganzfeld dome (0.001, 0.02, 0.25, 4.1, 137 cd s/m^2), and responses were recorded using a signal averaging system with bandpass filters set at 1 to 1500 Hz (BigShot; LKC Technologies, Gaithersburg, MD, USA).

Immunohistochemistry and Histology

To evaluate oxidized H-800CW in the ex vivo retina, rats were killed via pentobarbital overdose (100 mg/kg), immediately after the SLO examination at 2 days post LIRD. Mice were killed 7 days after LIRD to evaluate the effects of toxic light exposure. After enucleation, each eye was injected with fixative at the superior limbus and immersed in fixative solution (Z-fix; Anatech, Battle Creek, MI, USA) for 1 hour. Following dissection, the posterior eye cup was immersed in 30% sucrose until saturated. After freezing the tissue in tissue freezing medium (Tissue-Tek; Electron Microscopy Sciences, Hatfield, PA, USA), eye cups were cryosectioned at 10 μm (for immunohistochemistry) or 20 μm (for histology), collected on glass slides, and stored at −20°C. Sections including the optic nerve were stained with 4′,6-diamidino-2-phenylindole (DAPI; 1:1000), then coverslipped (ProLong Gold antifade reagent; Invitrogen, Eugene, OR, USA). Sections taken for histology were imaged with a phase-contrast light microscope (Leica, McHenry, IL, USA), and outer nuclear layer thickness measurements were taken. Sections taken for ex vivo oxidized H-800CW evaluation were imaged using a light microscope (EVOS FL Auto; Life Technologies, Carlsbad, CA, USA) under DAPI and Cy7 filters.

To ensure that H-800CW labels for oxidative stress, some sections were treated with 2′,7′-dichlorofluorescein diacetate (H2DCFDA; Life Technologies, Thermo Fisher Scientific, Waltham, MA, USA), which oxidizes to the fluorescent green compound DCF in the presence of cellular oxidation by peroxynitrite, hydrogen peroxide, and hydroxyl radicals.[51] Frozen retinal sections from hydrocyanine-injected eyes were incubated with H2DCFDA (10 μM) for 60 minutes at 37°C in the dark. Slides were treated with Vectashield (Vector Laboratories, Burlingame, CA, USA) and coverslipped. The DCF fluorescence was imaged using a light microscope (EVOS FL Auto, Life Technologies, Thermo Fisher Scientific) with green fluorescent protein filters.

Data Analysis

Using image analysis software (ImageJ; http://rsb.info.nih.gov/ij/ [in the public domain], Wayne Rasband, National Institutes of Health, Bethesda, MD, USA), we first converted one ICG image for each animal into an 8-bit grayscale image. For intensity measurement, we measured the average fluorescent intensity within a 150-pixel band surrounding the optic disc. Intensity comparisons were first normalized to the optic disc to account for background fluorescent noise. For area of hyperfluorescence, we first set a threshold value for each image within the same experiment, then converted to binary images of black (positive fluorescence: pixel exhibiting greater than the set threshold value) and white (negative fluorescence: pixel exhibiting less than set threshold value), and finally calculated the total area of pixels with positive fluorescence for each image.

All statistical analyses were performed using commercial software (SigmaStat 3.5; Aspire Software International, Ashburn, VA, USA). All data plotted in figures are represented as mean ± standard error of the mean (SEM). Statistical analysis included Student's *t*-test and repeated-measures analysis of variance (ANOVA) with Holm-Sidak post hoc tests for statistical significance at $P < 0.05$. When normality failed, the Mann-Whitney rank sum test or Kruskal-Wallis 1-way ANOVA on ranks was used. For systemic H-800CW injections, quantifications from SLOs were obtained from right eye images and were used as a representative of an individual animal. For intravitreally-injected H-800CW, eyes were considered independent and analyzed as such.

Results

LIRD Induces Retinal Damage in Pigmented Rodents

Since LIRD is typically performed in albino rodents,[52] we established that light damage can consistently induce retinal degeneration in pigmented 129/SvJ mice, based on previous methods (Chrenek, et al. *IOVS* 2013;54:ARVO E-Abstract 44). Mice exposed to toxic bright light (60,000 lux for 6 hours; LIRD) were compared to mice maintained in dim lighting (100 lux; CTRL) using OKT, ERG, and histology. Spatial frequency thresholds were significantly decreased in LIRD compared to CTRL mice (Fig. 2A; Student's *t*-test = 3.79, $P < 0.01$). Seven days post light exposure, ERG waveforms were visibly decreased in LIRD mice (Fig. 2B). Bright flash (4.1 cd s/m^2)-induced a- and b-wave amplitudes were significantly decreased by 65.7% and 62.5%, respectively, in LIRD mice compared to CTRL mice (Figs. 2B, 2C, a-wave: Mann-Whitney rank sum test = 4.0, $P = 0.01$, b-wave: Mann-Whitney rank sum test = 5.0, $P = 0.02$). Additionally, CTRL mice (Fig. 2D) had significantly thicker outer nuclear layers (ONL) than LIRD mice (Fig. 2E). Quantification of ONL thickness showed a 63% to 68% decrease superior to the optic nerve and a 48% decrease inferior to the optic nerve after bright light exposure (Fig. 2F; 2-way repeated ANOVA $F(3, 43) = 4.68$, $P = 0.009$). As expected, spatial frequency thresholds positively correlated

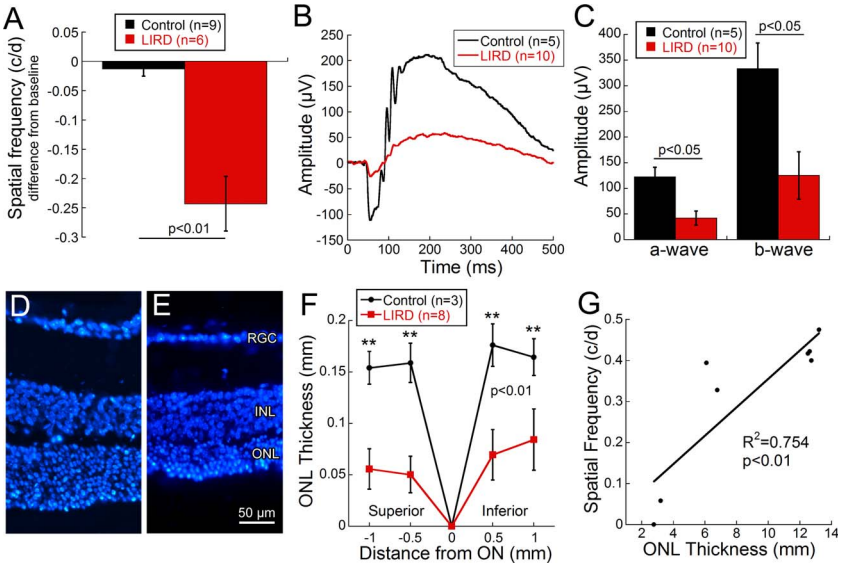

Figure 2. Behavioral, functional, and histologic analyses confirmed light-induced retinal damage in pigmented animals. Visual acuity decreased significantly from baseline in LIRD animals 6 days post light exposure ([**A**] Student's *t*-test = 3.79, $P < 0.01$). Averaged waveform (**B**) in response to bright-flash (4.1 cd s/m^2) stimulus from CTRL (*black*) and LIRD (*red*) 129/SvJ mice at 7 days post LIRD. Significant deficits in the absolute value of the a- and b-wave response occurred between CTRL and LIRD animals ([**C**] a-wave: Mann-Whitney rank sum test = 4.0, $P = 0.01$, b-wave: Mann-Whitney rank sum test = 5.0, $P = 0.02$). Measurements of DAPI-stained retinal cross sections confirmed thinning of the outer nuclear layer (ONL) thickness between CTRL (**D**) and LIRD (**E**) animals as quantified in (**F**). The ONL was significantly thinner in the LIRD mice compared to controls (2-way repeated ANOVA $F(3, 43) = 4.68$, $P = 0.009$). Visual acuity and ONL thickness are strongly correlated ([**G**] correlation $R^2 = 0.754$, $P < 0.01$), with reduction in ONL thickness corresponding to decreased visual acuity. Data shown are mean ± SEM. *Asterisks* represent significant post hoc comparisons, $^{**}P < 0.01$. RGC, retinal ganglion cell layer; INL, inner nuclear layer.

with ONL thickness (Fig. 2G, correlation $R^2 = 0.754$, $P < 0.01$) in pigmented 129/SvJ mice after LIRD.

Systemic Delivery of H-800CW Produces a Dose–Response Relationship

To assess the utility of systemically administered H-800CW to detect ROS, doses from 0 (vehicle only) to 20 mg/kg were intravenously delivered to both LIRD and CTRL mice. Since oxidized H-800CW fluorescence was similar across all doses in SLO fundus images of CTRL mice, CTRL mice were grouped as a single cohort. Light-induced retinal damage mice with vehicle also had the same appearance as CTRL mice, with only a small amount of fluorescence visible (see Fig. 3F), and were also grouped with the CTRL mice. In contrast, the pattern and appearance of oxidized H-800CW fluorescence changed with increasing doses in LIRD mice. Oxidized H-800CW diffusely permeated the retina around the optic nerve, producing low-level fluorescence (Figs. 3A–E). Fluorescein angiography was performed in both LIRD and CTRL animals after H-800CW administration and revealed that retinal vasculature was intact (Supplementary Fig. S1). Points of punctate hyperfluorescence became visible at the 5 mg/kg dose in LIRD mice and increased in size, quantity, and distance from the optic nerve with increasing doses (Figs. 3C–E, 3H–J). Neither diffuse nor punctate hyperfluorescence was visible in the CTRL animals (Figs. 3A, 2F). Mean oxidized H-800CW fluorescence in the fundus of LIRD animals increased in direct relation to concentration of injected H-800CW, reaching statistical significance at concentrations of 10 mg/kg and above (Figs. 3D, 3E) when compared to CTRL mice (Figs. 3A, 3L; Kruskal-Wallis 1-way ANOVA on ranks, $H = 23.4$, $P < 0.001$). Converted binary color images emphasized areas of increased fluorescence (Figs. 3F–J). Similar to calculations of mean fluorescence, hyperfluorescent area in the fundi of LIRD mice was greater than in CTRL mice at doses of 10 or 20 mg/kg (Fig. 3M; Kruskal-Wallis 1-way ANOVA on ranks, $H = 23.6$, $P < 0.001$). The dose–response relationship for H-800CW was nearly linear for both mean fluorescence ($R^2 = 0.705$) and hyperfluorescence area ($R^2 = 0.796$). Additionally, the values of mean fluorescence and fluorescent area were highly correlated between the two quantification methods ($R^2 = 0.935$, $P < 0.001$; Fig. 3N), suggesting that either may be appropriate for quantification in future experiments.

H-800CW Is Sensitive to the Amount of Retinal Damage

By varying the duration of toxic light exposure, we determined H-800CW's response to increasing retinal damage. Immediately after 0 (CTRL), 1, 2, 4, and 6 hours of light exposure, animals were intravenously injected with 20 mg/kg H-800CW. As the duration of toxic light exposure increased, the mean fluorescence (Figs. 4A–E) and total fluorescent area (Figs. 4F–J) also increased. However, only the mice subjected to 4 and 6 hours of LIRD yielded significantly higher mean fluorescence values than CTRL mice (Fig. 4K; Kruskal-Wallis 1-way ANOVA on ranks, $H = 16.17$, $P = 0.003$). All mice that received toxic light exposure exhibited significantly greater fluorescent area than CTRL mice (Fig. 4L; 1-way ANOVA $F(4, 20) = 21.68$, $P < 0.001$). Comparisons of hyperfluorescent areas also showed significant differences between 1 and 4 to 6 hours and 2 and 6 hours of light exposure (Fig. 4L; $P < 0.01$). Fluorescent area and mean fluorescence were significantly correlated ($R^2 = 0.793$, $P < 0.001$). However, fluorescent area was more sensitive to light exposure than fluorescent intensity.

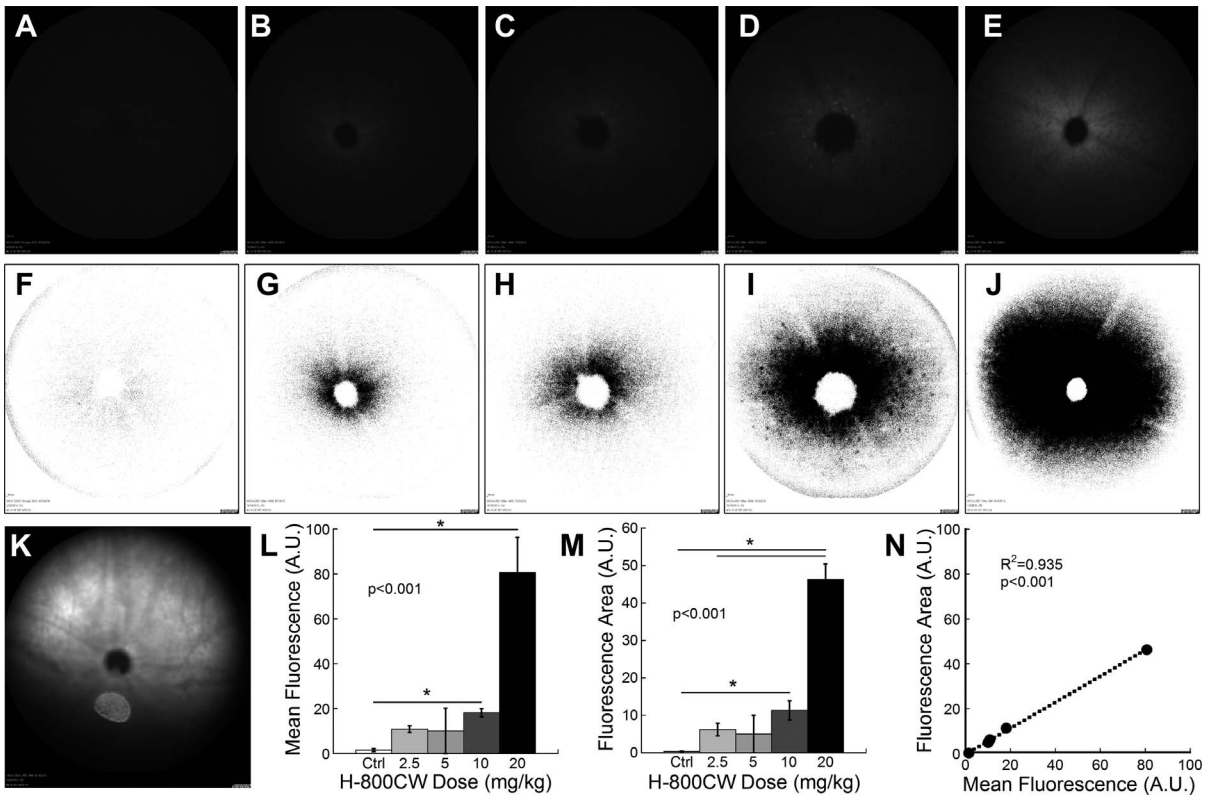

Figure 3. Representative fundus images of 129/SvJ mice after LIRD showing the dose–response curve for intravenous H-800CW. Hyperfluorescence of oxidized H-800CW is shown in the fundus using SLO (**A**–**E**) or as fundus images with converted colors to show the area of hyperfluorescence (**F**–**J**). CTRL (**A**, **F**) or LIRD animals received a dose of 2.5 ($n = 7$; [**B**, **G**]), 5 ($n = 4$; [**C**, **H**]), 10 ($n = 7$; [**D**, **I**]), or 20 mg/kg ($n = 5$; [**E**, **J**]) H-800CW. All CTRL mice receiving any H-800CW dose and LIRD mice receiving vehicle appeared the same as shown in (**A**). Mean fluorescent intensity was significantly greater with 10 or 20 mg/kg doses ([**L**] Kruskal-Wallis 1-way ANOVA on ranks, $H = 23.4$, $P < 0.001$). The total area of positive fluorescence was significantly greater in mice receiving the two highest doses ([**M**] Kruskal-Wallis 1-way ANOVA on ranks, $H = 23.6$, $P < 0.001$). A representative IR fundus image (**K**) showing the plane of focus for the ICG fluorescent images shown in (**A**–**E**). Oxidized H-800CW fluorescence was located distal to the retinal vasculature. The two methods of fluorescent quantification show highly correlated measurements (**N**). Post hoc comparisons *$P < 0.05$.

Oxidized H-800CW Fluorescence Significantly Correlates With Visual Function

To determine if ROS level correlated with visual dysfunction as detected by oxidized H-800CW fluorescence, we plotted visual acuity (spatial frequency threshold) against mean fluorescent intensity in LIRD mice administered 10 mg/kg H-800CW. Mean fluorescence was greater in mice with lower visual acuity (Fig. 5; correlation $R^2 = 0.616$, $P = 0.001$), which suggests that mice with greater visual deficits, and presumably greater ROS production, have increased H-800CW binding in the fundus images. Importantly, the spatial frequency thresholds of CTRL mice injected with H-800CW (0.45 ± 0.01 cyc/deg) did not differ from those in 8-week-old naïve 129SV mice (0.45 ± 0.004 cyc/deg; Student's *t*-test $P = 0.59$), suggesting no toxic effects of H-800CW to the retinal function.

Oxidized H-800CW Localizes to Retinal Photoreceptors

Long Evans rats were intravitreally injected with H-800CW and imaged with the ICG filter of the SLO. Minimal baseline fluorescence was visible in the fundus image of the CTRL rats injected with H-800CW (Fig. 6A). In comparison, LIRD rats (Fig. 6B) showed oxidized H-800CW hyperfluorescence in the fundus with both punctate and diffuse patterns. The distinct ring of fluorescence around the optic nerve was observed in all LIRD rat fundus images with intravitreal injections of H-800CW. The crescent-shaped area of hyperfluorescence in the superior quadrant of the LIRD fundus may be a result of the H-800CW injection to the superior limbus, which could saturate the superior retina and bind to all available ROS. Fluorescence was visualized deep in the retinal layers but before the choroidal vessels, as indicated by the focal plane of the infrared (IR) fundus image in Figure 6C.

Using DAPI-labeled retinal sections, oxidized H-800CW was undetectable in CTRL rats (Fig. 7B). Note that the typical 12 or 13 rows of ONL nuclei are visible in the CTRL rat treated with H-800CW, suggesting no adverse effects of the dye on retinal structure. However, retinas from LIRD rats showed significant oxidized H-800CW in the inner segments of the photoreceptors and ONL (Figs. 7D–F). A low-magnification image from an LIRD rat injected with H-800CW shows the breadth and localization of oxidized H-800CW within the retina (Fig. 7F).

To further validate H-800CW as a marker for sites of ROS production, retinal sections from H-800CW-injected rats were colabeled with DCF. Dichlorofluorescein most strongly labels the photoreceptor inner segments and outer plexiform layer (OPL) with diffuse labeling in the remaining retinal layers (Fig. 7G). Similarly, oxidized H-800CW fluorescence was specific to the photoreceptor inner segments, ONL, and OPL (Figs. 7H, 7I).

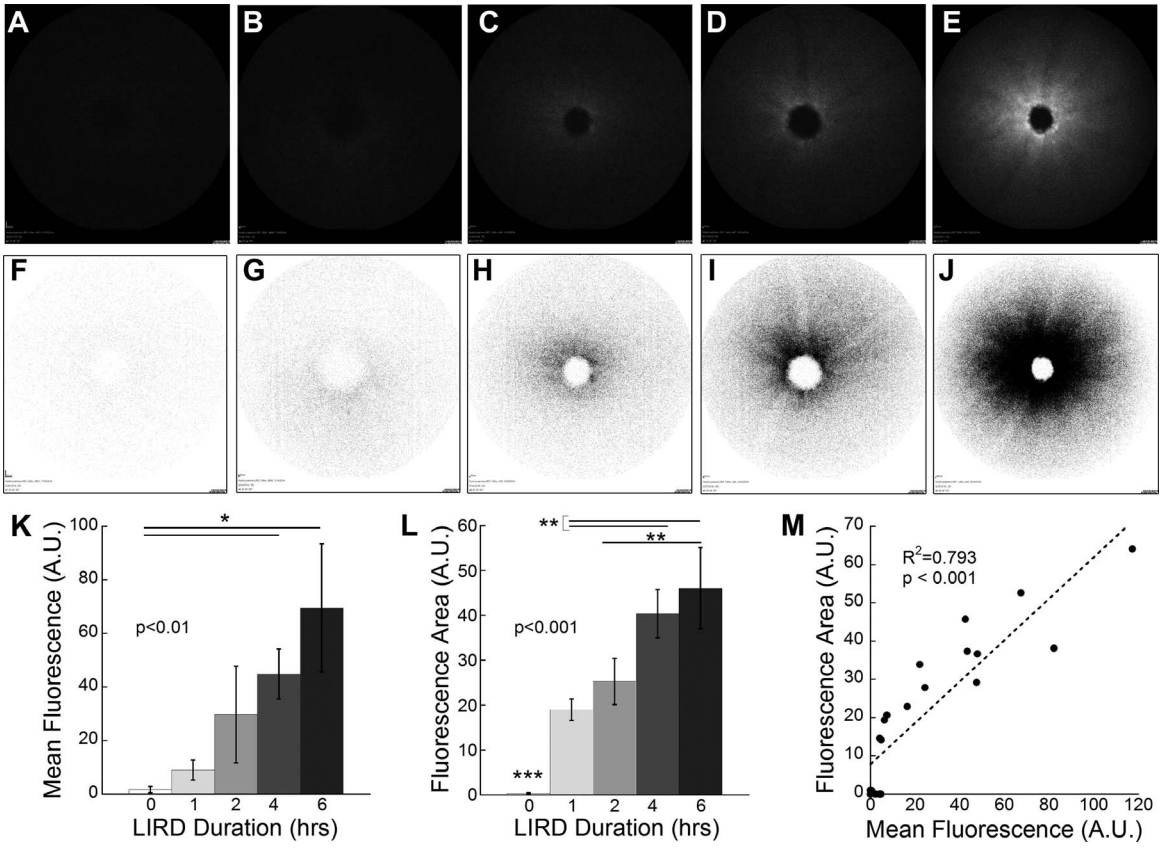

Figure 4. Representative fundus images of 129/SvJ mice exposed to increasing durations of light toxicity after intravenous H-800CW injections. Animals were subjected to 60,000 lux light for durations of 0 (CTRL; $n = 7$; [**A**, **F**]), 1 ($n = 3$; [**B**, **G**]), 2 ($n = 4$; [**C**, **H**]), 4 ($n = 4$; [**D**, **I**]), and 6 ($n = 3$; [**E**, **J**])) hours. Mean fluorescence was measured (**K**) from the images obtained with SLO (**A**–**E**). Animals subjected to light damage for 4 and 6 hours yielded mean fluorescence values that were significantly greater than in CTRL animals ([**K**] Kruskal-Wallis 1-way ANOVA on ranks, $H = 16.17$, $P = 0.003$). Area of hyperfluorescence was measured from color inverted SLO images (**F**–**J**). Hyperfluorescence area was significantly greater in all mice exposed to toxic light compared to CTRL (0 hours; [**L**] 1-way ANOVA $F(4, 20) = 21.68$, $P < 0.001$). Additionally, significant differences were found between mice exposed to increasing toxic light, illustrating the sensitivity of H-800CW to detect ROS levels with increasing retinal damage. Quantification by area or intensity was highly correlated with area of hyperfluorescence showing greater sensitivity (**M**). Post hoc comparisons $^{*}P < 0.05$, $^{**}P < 0.01$, $^{***}P < 0.001$.

Discussion

H-800CW Enables In Vivo Detection of ROS in Retinal Degeneration

We tested whether H-800CW administration can detect ROS in the LIRD model of retinal degeneration using fundoscopic in vivo SLO imaging. Our results show that oxidized H-800CW mean fluorescence and fluorescent area increased in a dose-dependent fashion and increased across a range of retinal damage. Both parameters can be reliably quantified in the retina. Furthermore, we localized oxidized H-800CW hyperfluorescence to photoreceptors, the expected location of ROS generation in the LIRD model,[41] and confirmed that oxidized H-800CW had similar labeling patterns to another commonly used ROS marker, DCF.[26] Importantly, oxidized H-800CW fluorescence and fluorescent area correlated with visual dysfunction in the pigmented LIRD model used here (Fig. 5). While differences in H-800CW fluorescence accounted for only 61% of the change in spatial frequency threshold, this significant correlation suggests a relationship between ROS-activated fluorescence and visual function and therefore indicates the potential clinical relevance of this diagnostic approach in pigmented human eyes.

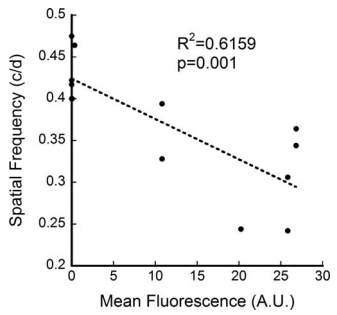

Figure 5. In vivo oxidized H-800CW fluorescence correlates with visual function. Within the cohort of 129/SvJ mice that received the 10 mg/kg dose of H-800CW, animals with worse visual acuity showed higher oxidized H-800CW fluorescence values in the fundus.

Oxidized H-800CW Has a Consistent Appearance and Location in the Retina

The pattern of oxidized H-800CW fluorescence increased dramatically as the dose of H-800CW increased from 2.5 to 20 mg/kg in LIRD animals. Higher doses of H-800CW extended further from the optic nerve with the fluorescent intensity decreasing with distance from the optic nerve. These punctate complexes could be apoptotic cells being phagocytosed by macrophages or ROS conglomerates that are created during

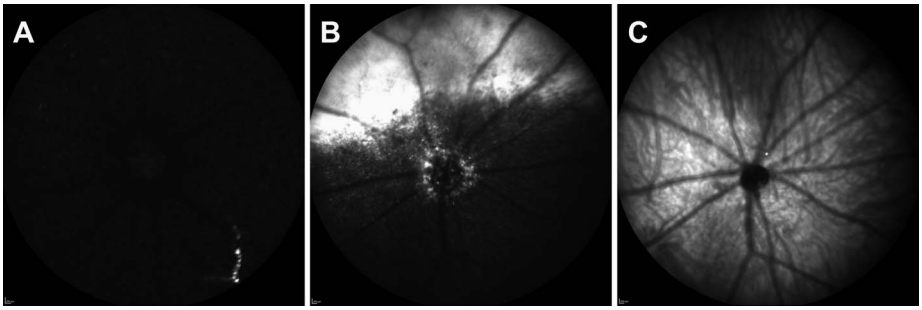

FIGURE 6. Fundus imaging of CTRL (**A**) and LIRD (**B**) Long Evans rats that received intravitreal injection of H-800CW in the superior limbus. A representative IR fundus image (**C**) coplanar to ICG fluorescent images (**A**, **B**) is included to show that fluorescence was located deep within the retina, but anterior to the choroidal vessels.

photoreceptor phagocytosis by the RPE.[53] However, when retinal cross sections were examined, oxidized H-800CW was concentrated in the ONL and inner segments of the photoreceptors, not in the RPE (Figs. 7C–F). Since LIRD causes photoreceptor apoptosis,[52] ROS localization was expected in this location and is consistent with previous reports of oxidative stress in LIRD that have shown high levels of ROS in the inner and outer segments of retinal rod photoreceptors.

Hydrocyanine-800CW belongs to a family of ROS dyes referred to as hydrocyanines, which can be engineered to have intra- or extracellular properties.[30] Hydrocyanine-800CW was developed as an extracellular dye. Thus, intravenous injections would be expected to react with ROS in extracellular fluid, including within the blood vessels. However, the H-800CW may have translocated intracellularly in light-damaged animals since the fluorescence appears in the inner segments (Fig. 7D). Since oxidative stress can damage the integrity of the cell's plasma membrane,[54] H-800CW may have permeated the cell membrane after severe light damage. Additionally, SLO fundus images showed the oxidized H-800CW dye to be predominantly located in the area immediately around the optic nerve.

H-800CW Is a Suitable Biomarker for Ocular ROS

While hydrocyanines have previously been used in models of septic shock,[30] stroke, [20] inflammation,[31,34–36,38] and osteoarthritis,[39] this study is the first to report its potential for ophthalmic uses. In preparation for clinical trials, an oxidized version of the probe (IRDye 800 CW) is being manufactured with current good manufacturing practices (cGMP; www.licor.com [in the public domain]), has a drug master file with the Food and Drug Administration (www.licor.com), has an active substance master file with European Medicines Agency (www.licor.com), and has exhibited negative results for toxicity.[55] Oxidized H-800CW also has good stability after binding to ROS, as the 800CW-ROS complexes were still visible 48 hours after injection (although our animals were kept in the dark). Though hydrocyanines have various excitation and emission wavelengths,[30] H-800CW's excitation (774 nm) and emission (789 nm) wavelengths make

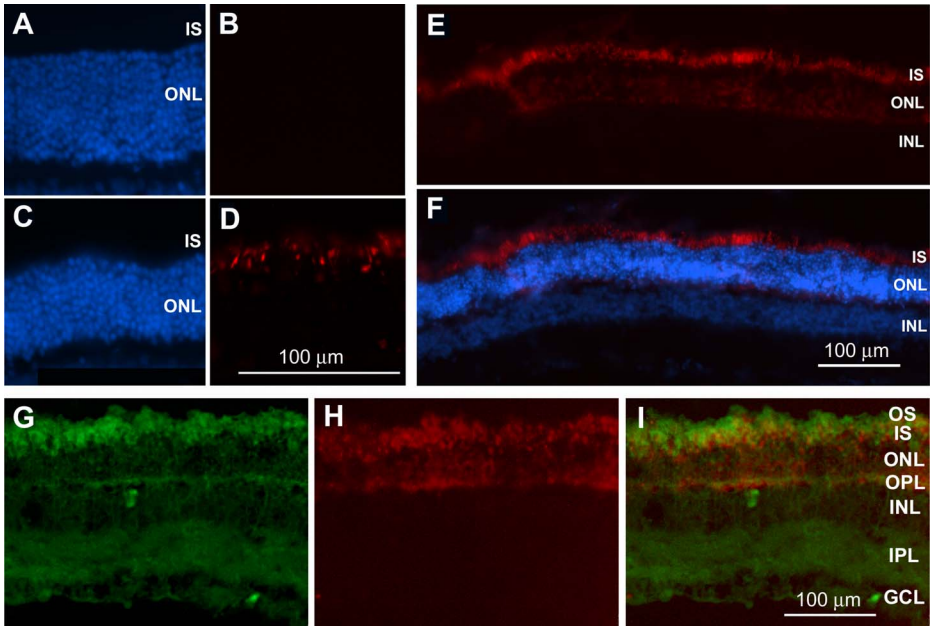

FIGURE 7. Representative micrographs from retinal sections of Long Evans rats that were intravitreally injected with H-800CW (*red*) in vivo. DAPI staining (*blue*) in CTRL (**A**) and LIRD (**C**) retinas enabled visualization of retinal layers. Oxidized H-800CW fluorescence was absent from CTRL retinas (**B**) but strongly labeled the inner segments (IS) and outer nuclear layer (ONL) of LIRD retinas (**D**). A lower-magnification image of the retina showing consistent ROS labeling localized within the IS and ONL (**E**, **F**). Dichlorofluorescein labeling ([**G**] *green*) of retinas from H-800CW-injected eyes ([**H**] *red*) shows colabeling in the photoreceptor inner segments, outer nuclear layer, and outer plexiform layer (**I**), confirming that oxidized H-800CW labels ROS. OS, outer segments; IS, inner segments; INL, inner nuclear layer; IPL, inner plexiform layer; GCL, ganglion cell layer.

it particularly compatible with the ICG filter of commonly available SLO instruments found in most ophthalmology and optometry offices. Thus, H-800CW could easily be translated into clinical use with existing ophthalmic instruments. The current results did not reach a plateau for dose–response curve (Fig. 3) or retinal damage (Fig. 4), suggesting that H-800CW can be further optimized. This in vivo ROS probe for the retina enables direct measurement of superoxide and hydroxyl radical levels, allowing individual patients to be tracked longitudinally and improving knowledge about ocular disease progression. Hydrocyanine-800CW also provides an in vivo research tool for preclinical retinal studies, without the need for ex vivo ROS quantification from retinal biopsies.

Acknowledgments

Supported by Department of Veterans Affairs Rehab R&D Merit Award E0951-R (MTP) and Research Career Scientist Award C6774S (MTP), National Institutes of Health (NIH) EY016435 (MTP), NIH R01 EY014026 (JHB), NIH P30 EY006360, departmental grant from Research to Prevent Blindness, and a grant from the Abraham J. and Phyllis Katz Foundation (JHB).

Disclosure: **M.C. Prunty**, None; **M.H. Aung**, None; **A.M. Hanif**, None; **R.S. Allen**, None; **M.A. Chrenek**, None; **J.H. Boatright**, None; **P.M. Thule**, None; **K. Kundu**, LI-COR (E), P; **N. Murthy**, P; **M.T. Pardue**, None

References

1. Blasiak J, Petrovski G, Vereb Z, Facsko A, Kaarniranta K. Oxidative stress, hypoxia, and autophagy in the neovascular processes of age-related macular degeneration. *Biomed Res Int*. 2014;2014:768026.
2. Kiang AS, Humphries MM, Campbell M, Humphries P. Antioxidant therapy for retinal disease. *Adv Exp Med Biol*. 2014;801:783–789.
3. Pinazo-Duran MD, Zanon-Moreno V, Garcia-Medina JJ, Gallego-Pinazo R. Evaluation of presumptive biomarkers of oxidative stress, immune response and apoptosis in primary open-angle glaucoma. *Curr Opin Pharmacol*. 2013;13:98–107.
4. Elahy M, Baindur-Hudson S, Cruzat VF, Newsholme P, Dass CR. Mechanisms of PEDF-mediated protection against reactive oxygen species damage in diabetic retinopathy and neuropathy. *J Endocrinol*. 2014;222:R129–R139.
5. Williams M, Hogg RE, Chakravarthy U. Antioxidants and diabetic retinopathy. *Curr Diab Rep*. 2013;13:481–487.
6. Payne AJ, Kaja S, Naumchuk Y, Kunjukunju N, Koulen P. Antioxidant drug therapy approaches for neuroprotection in chronic diseases of the retina. *Int J Mol Sci*. 2014;15:1865–1886.
7. Maleki S, Gopalakrishnan S, Ghanian Z, et al. Optical imaging of mitochondrial redox state in rodent model of retinitis pigmentosa. *J Biomed Opt*. 2013;18:16004.
8. Kutty RK, Kutty G, Wiggert B, Chader GJ, Darrow RM, Organisciak DT. Induction of heme oxygenase 1 in the retina by intense visible light: suppression by the antioxidant dimethylthiourea. *Proc Natl Acad Sci U S A*. 1995;92:1177–1181.
9. Organisciak DT, Vaughan DK. Retinal light damage: mechanisms and protection. *Prog Retin Eye Res*. 2010;29:113–134.
10. Pinazo-Duran MD, Gallego-Pinazo R, Garcia-Medina JJ, et al. Oxidative stress and its downstream signaling in aging eyes. *Clin Interv Aging*. 2014;9:637–652.
11. Komeima K, Rogers BS, Campochiaro PA. Antioxidants slow photoreceptor cell death in mouse models of retinitis pigmentosa. *J Cell Physiol*. 2007;213:809–815.
12. Boatright JH, Moring AG, McElroy C, et al. Tool from ancient pharmacopoeia prevents vision loss. *Mol Vis*. 2006;12:1706–1714.
13. Osborne NN, del Olmo-Aguado S. Maintenance of retinal ganglion cell mitochondrial functions as a neuroprotective strategy in glaucoma. *Curr Opin Pharmacol*. 2013;13:16–22.
14. Lee D, Kim KY, Shim MS, et al. Coenzyme Q10 ameliorates oxidative stress and prevents mitochondrial alteration in ischemic retinal injury. *Apoptosis*. 2014;19:603–614.
15. Pitocco D, Tesauro M, Alessandro R, Ghirlanda G, Cardillo C. Oxidative stress in diabetes: implications for vascular and other complications. *Int J Mol Sci*. 2013;14:21525–21550.
16. Liu Q, Ju WK, Crowston JG, et al. Oxidative stress is an early event in hydrostatic pressure induced retinal ganglion cell damage. *Invest Ophthalmol Vis Sci*. 2007;48:4580–4589.
17. Du Y, Veenstra A, Palczewski K, Kern TS. Photoreceptor cells are major contributors to diabetes-induced oxidative stress and local inflammation in the retina. *Proc Natl Acad Sci U S A*. 2013;110:16586–16591.
18. Arden GB, Sivaprasad S. The pathogenesis of early retinal changes of diabetic retinopathy. *Doc Ophthalmol*. 2012;124:15–26.
19. Frost SM, Kanagasingam Y, Macaulay SL. Ocular biomarkers for neurodegenerative and systemic disease. *Med J Aust*. 2014;201:128.
20. Schoknecht K, Prager O, Vazana U, et al. Monitoring stroke progression: in vivo imaging of cortical perfusion, blood-brain barrier permeability and cellular damage in the rat photothrombosis model. *J Cereb Blood Flow Metab*. 2014;34:1791–1801.
21. Allen RS, Sayeed I, Cale HA, et al. Severity of middle cerebral artery occlusion determines retinal deficits in rats. *Exp Neurol*. 2014;254:206–215.
22. Frost S, Martins RN, Kanagasingam Y. Ocular biomarkers for early detection of Alzheimer's disease. *J Alzheimers Dis*. 2010;22:1–16.
23. Tas A, Yolcu U, Ilhan A, Gundogan FC. Detection of retinal nerve fibre layer degeneration in patients with Alzheimer's disease using optical coherence tomography: searching new biomarkers (published online ahead of print December 9, 2014). *Acta Ophthalmol*. doi:10.1111/aos.12614.
24. Blake R, Trounce IA. Mitochondrial dysfunction and complications associated with diabetes. *Biochim Biophys Acta*. 2014;1840:1404–1412.
25. Giorgio M, Trinei M, Migliaccio E, Pelicci PG. Hydrogen peroxide: a metabolic by-product or a common mediator of ageing signals? *Nat Rev Mol Cell Biol*. 2007;8:722–728.
26. Park SW, Cho CS, Jun HO, et al. Anti-angiogenic effect of luteolin on retinal neovascularization via blockade of reactive oxygen species production. *Invest Ophthalmol Vis Sci*. 2012;53:7718–7726.
27. Zielonka J, Vasquez-Vivar J, Kalyanaraman B. Detection of 2-hydroxyethidium in cellular systems: a unique marker product of superoxide and hydroethidine. *Nat Protoc*. 2008;3:8–21.
28. Pritsos CA, Constantinides PP, Tritton TR, Heimbrook DC, Sartorelli AC. Use of high-performance and superoxide liquid chromatography to detect hydroxyl radicals generated from mitomycin C. *Anal Biochem*. 1985;150:294–299.
29. Rayner CL, Gole GA, Bottle SE, Barnett NL. Dynamic, in vivo, real-time detection of retinal oxidative status in a model of elevated intraocular pressure using a novel, reversibly responsive, profluorescent nitroxide probe. *Exp Eye Res*. 2014;129:48–56.
30. Kundu K, Knight SF, Willett N, Lee S, Taylor WR, Murthy N. Hydrocyanines: a class of fluorescent sensors that can image

reactive oxygen species in cell culture, tissue, and in vivo. *Angew Chem Int Ed Engl*. 2009;48:299–303.

31. Lin PW, Myers LE, Ray L, et al. Lactobacillus rhamnosus blocks inflammatory signaling in vivo via reactive oxygen species generation. *Free Radic Biol Med*. 2009;47:1205–1211.
32. Willett NJ, Kundu K, Knight SF, Dikalov S, Murthy N, Taylor WR. Redox signaling in an in vivo murine model of low magnitude oscillatory wall shear stress. *Antioxid Redox Signal*. 2011;15:1369–1378.
33. Dinjaski N, Fernandez-Gutierrez M, Selvam S, et al. PHACOS, a functionalized bacterial polyester with bactericidal activity against methicillin-resistant Staphylococcus aureus. *Biomaterials*. 2014;35:14–24.
34. Selvam S, Kundu K, Templeman KL, Murthy N, Garcia AJ. Minimally invasive, longitudinal monitoring of biomaterial-associated inflammation by fluorescence imaging. *Biomaterials*. 2011;32:7785–7792.
35. Suri S, Lehman SM, Selvam S, et al. In vivo fluorescence imaging of biomaterial-associated inflammation and infection in a minimally invasive manner. *J Biomed Mater Res A*. 2015; 103:76–83.
36. Magalotti S, Gustafson TP, Cao Q, et al. Evaluation of inflammatory response to acute ischemia using near-infrared fluorescent reactive oxygen sensors. *Mol Imaging Biol*. 2013; 15:423–430.
37. Goodson P, Kumar A, Jain L, et al. Nadph oxidase regulates alveolar epithelial sodium channel activity and lung fluid balance in vivo via O(-)(2) signaling. *Am J Physiol Lung Cell Mol Physiol*. 2012;302:L410–L419.
38. Kim JY, Choi WI, Kim YH, Tae G. Highly selective in-vivo imaging of tumor as an inflammation site by ROS detection using hydrocyanine-conjugated, functional nano-carriers. *J Control Release*. 2011;156:398–405.
39. Xie L, Lin AS, Kundu K, Levenston ME, Murthy N, Guldberg RE. Quantitative imaging of cartilage and bone morphology, reactive oxygen species, and vascularization in a rodent model of osteoarthritis. *Arthritis Rheum*. 2012;64:1899–1908.
40. Kundu K, Knight SF, Lee S, Taylor WR, Murthy N. A significant improvement of the efficacy of radical oxidant probes by the kinetic isotope effect. *Angew Chem Int Ed Engl*. 2010;49: 6134–6138.
41. Demontis GC, Longoni B, Marchiafava PL. Molecular steps involved in light-induced oxidative damage to retinal rods. *Invest Ophthalmol Vis Sci*. 2002;43:2421–2427.
42. Turner PV, Albassam MA. Susceptibility of rats to corneal lesions after injectable anesthesia. *Comp Med*. 2005;55:175–182.
43. Guillet R, Wyatt J, Baggs RB, Kellogg KC. Anesthetic-induced corneal lesions in developmentally sensitive rats. *Invest Ophthalmol Vis Sci*. 1988;29:6:949–954.
44. Seeliger MW, Beck SC, Pereyra-Munoz N, et al. In vivo confocal imaging of the retina in animal models using scanning laser ophthalmoscopy. *Vision Res*. 2005;45:3512–3519.
45. Prusky GT, Alam NM, Beekman S, Douglas RM. Rapid quantification of adult and developing mouse spatial vision using a virtual optomotor system. *Invest Ophthalmol Vis Sci*. 2004;45:4611–4616.
46. Prusky GT, West PW, Douglas RM. Behavioral assessment of visual acuity in mice and rats. *Vision Res*. 2000;40:2201–2209.
47. Aung MH, Kim MK, Olson DE, Thule PM, Pardue MT. Early visual deficits in streptozotocin-induced diabetic long evans rats. *Invest Ophthalmol Vis Sci*. 2013;54:1370–1377.
48. Aung MH, Park HN, Han MK, et al. Dopamine deficiency contributes to early visual dysfunction in a rodent model of type 1 diabetes. *J Neurosci*. 2014;34:726–736.
49. Lawson EC, Han MK, Sellers JT, et al. Aerobic exercise protects retinal function and structure from light-induced retinal degeneration. *J Neurosci*. 2014;34:2406–2412.
50. Mocko JA, Kim M, Faulkner AE, Cao Y, Ciavatta VT, Pardue MT. Effects of subretinal electrical stimulation in mer-KO mice. *Invest Ophthalmol Vis Sci*. 2011;52:4223–4230.
51. Munzel T. Detection of superoxide in vascular tissue. *Arterioscler Thromb Vasc Biol*. 2002;22:1761–1768.
52. Noell WK, Walker VS, Kang BS, Berman S. Retinal damage by light in rats. *Invest Ophthalmol Vis Sci*. 1966;5:450–473.
53. Kevany BM, Palczewski K. Phagocytosis of retinal rod and cone photoreceptors. *Physiology (Bethesda)*. 2010;25:8–15.
54. Zarebski M, Kordon M, Dobrucki JW. Photosensitized damage inflicted on plasma membranes of live cells by an extracellular generator of singlet oxygen—a linear dependence of a lethal dose on light intensity. *Photochem Photobiol*. 2014;90:709–715.
55. Marshall MV, Draney D, Sevick-Muraca EM, Olive DM. Single-dose intravenous toxicity study of IRDye 800CW in Sprague-Dawley rats. *Mol Imaging Biol*. 2010;12:583–594.

Investigative Ophthalmology & Visual Science